Cement & Concrete Composites 39 (2013) 1–11

Contents lists available at SciVerse ScienceDirect

Cement & Concrete Composites

journal homepage: www.elsevier.com/locate/cemconcomp

Dynamic behavior of porous concretes under drop weight impact testing

Ayda S. Agar Ozbek [a,*], Jaap Weerheijm [b,c], Erik Schlangen [a], Klaas van Breugel [a]

[a] Section of Materials and Environment – Microlab, Faculty of Civil Engineering and Geosciences, Delft University of Technology, 2628 CN Delft, The Netherlands
[b] TNO, Defence Security and Safety, Rijswijk, The Netherlands
[c] Section of Structural Mechanics, Faculty of Civil Engineering and Geosciences, Delft University of Technology, 2628 CN Delft, The Netherlands

ARTICLE INFO

Article history:
Received 7 July 2011
Received in revised form 19 March 2013
Accepted 21 March 2013
Available online 1 April 2013

Keywords:
Porous concrete
Drop weight impact
Dynamic testing
Laser Doppler velocimetry

ABSTRACT

Porous concrete is used as a construction material in various applications mainly as a permeable cementitious material. However, its response under impact loading is generally not considered. Due to the high percentage of its intentional meso-size air pores, porous concrete has a moderate static strength compared to normal concrete while its dynamic performance is distinctive. Owing to its characteristic of forming multiple cracks, it fractures into small fragments when exposed to impact loading. Therefore, with the aim of designing a special type of concrete to be used in protective structures, porous concrete was investigated. In this study, the impact strengths of different types of porous concretes were analyzed in correlation with their mixture compositions and production technique. The dynamic experiments were performed using a drop weight impact test set-up while the measurements were taken through Laser Doppler velocimetry. According to the results obtained, the aggregate properties and compactive effort, which are coupled to porosity, are the main factors that affect the dynamic performance of porous concrete.

1. Introduction

Porous concrete is a special type of cementitious material composed of gap graded aggregates, covered with a thin layer of cement paste, assembled by the cement paste layers partially being in contact. Porous concrete incorporates a high amount of intentionally included air voids that makes its physical characteristics markedly differ from normal concrete. Therefore, it is currently being used in various applications that require permeability, noise absorption or thermal insulation [1–4]. Due to its high intentional meso-size air pore content, porous concrete has a moderate static strength compared to normal concrete while its fragmentation behavior under dynamic loading is considerably different from that of normal concrete.

A research project was undertaken aiming to design a special type of cementitious material that fractures into small fragments under impact loading, to be used in protective structures such as safety walls for important structures such as embassies or storages for explosives. The purpose behind investigating the possibilities of making such a concrete that fractures into small fragments is the fact that in case of an explosion, the large fragments of concrete that are formed can also be fatal for the exposed environment. Due to its high intentional meso-size air pore content, porous concrete has a moderate static strength compared to normal concrete while its fragmentation behavior under dynamic loading is considerably different from that of normal concrete. Therefore, it was investigated in the scope of this research. In cementitious materials that also contain aggregate inclusions, microcracks typically initiate from the aggregate-cement paste interface due to high stress concentrations caused by the stiffness mismatch between the aggregates and the cementitious phases, as well as the weak interfacial bonding. These microcracks propagate and coalesce under increased loading. Under dynamic compressive loading, failure happens as a result of ultimate coalescence of these cracks. Because these cracks produce the post-failure fragments, the fragment size is directly related to how the cracks are distributed at coalescence [5–7]. In porous concrete, the initiation of the cracks is expected to be similar to that of normal concrete. However, because there is a very high amount of intentional voids present and because the cement paste bridges that bond coarse aggregates are very thin, the cracking patterns are affected by the geometry of the present phases. Therefore, porous concrete tends to fail at these numerous weak bridges between the aggregates which makes its ultimate behavior different from normal concrete. The fragments after an impact test being small in size can be explained by the presence of these weak bridges. Because pores are essential for the required dynamic performance of the material, in the process of modifying the mixture components, the main focus was to en-

* Corresponding author.
E-mail addresses: aydasafakagar@gmail.com (A.S. Agar Ozbek), jaap.weerheijm@tno.nl, J.Weerheijm@tudelft.nl (J. Weerheijm), H.E.J.G.Schlangen@tudelft.nl (E. Schlangen), K.vanBreugel@tudelft.nl (K. van Breugel).

0958-9465/$ - see front matter © 2013 Elsevier Ltd. All rights reserved.
http://dx.doi.org/10.1016/j.cemconcomp.2013.03.012

hance the static strength while maintaining a sufficient level of porosity. In porous concrete, the void content can be adjusted by modifying the aggregate proportions and properties as well as the level of compactive effort while the lack of fine aggregates is the main reason behind the enhanced void structure [8].

In order to produce porous concretes with the aimed static and impact strengths and to have reproducible results, all the important parameters have to be well-controlled. Therefore, the properties such as aggregate grading and characteristics and the compactive effort which are very effective on the ultimate material properties, have to be clearly elaborated. The aggregate properties influence the workability and the rheological properties of normal concrete as well as porous concrete. It is commonly accepted for normal concrete that well graded aggregates having particles of a wide range of sizes increase workability as they generally facilitate the flow of particles up to a threshold, provided that there is a sufficient amount of cement paste with a suitable workability present in the mixture [9]. As the aggregate grading affects the packing of particles, it also influences the efficiency of compaction because small particles are manipulated more efficiently into the voids between the larger ones [10]. Size of the particles also influences the properties of porous concrete in the sense that it is one of the main factors that control the pore size distribution such that an increase in aggregate size results in an increased median pore size. This effect is easily observable in mixtures with single sized aggregates. However, it should also be noted that there is no significant difference in the total pore volume between mixtures containing single-sized aggregates in different sizes where a porosity of typically between 21% and 24% can be expected [4]. Morphological properties of aggregates also affect the rheology and the mechanical properties of normal and porous concretes. Rounded aggregates provide a lower viscosity than angular ones and result in an increased packing. The flakiness is more likely to cause the particles to be oriented in one plane under compaction force. However, increased texture and enhanced angularity contribute to concrete strength due to two considerable factors which are particle-to-particle mechanical interlock and increased total surface area available for the adherence of the cement paste [9,11]. The different mechanical properties of the aggregates also have an influence on the strength of porous concrete even for aggregates that have the same texture [11]. Because the workability of fresh porous concrete is highly lowered, compaction is essential during casting. Meanwhile, the effect of prolonged compaction time causes a significant decrease in workability and a corresponding decline in compactibility due to the initiation of setting in the cement paste and moisture loss at the high amount of air exposed surface of porous concrete [8,12]. Therefore, the admixtures used in a porous concrete mixture should be precisely adjusted.

In this experimental study, impact strengths of different types of porous concretes with varying mixture compositions and production techniques were tested. The effects of different factors on the properties of porous concrete were investigated. Dynamic experiments were performed using a drop weight impact test set-up utilizing Laser Doppler velocimetry (LDV) as the monitoring technique. LDV is a diagnostic technique for measuring the velocity based on the Doppler principle of monitoring the change in the wavelength of the reflected laser light as a function of the relative velocity of a moving object [13]. While LDV has been used in applications where different materials have been tested under dynamic loading [14–16], drop weight impact testing is used in studies where dynamic performance of cementitious materials is investigated [17,18]. In the current study, LDV has been selected to be used in monitoring the particle velocity history of the impactor surface at the interface between the impactor and the concrete targets. During the drop weight impact experiments, the failure patterns were also monitored through high speed photography while the post-failure fragments were analyzed in terms of their sizes [19].

2. Experimental investigations

2.1. Materials

In order to achieve a highly porous structure, both the mixture design and the casting procedure of porous concrete have to differ from those of normal concrete. In the porous concrete mixtures produced in this study, aggregates were either at one (2–4 mm or 4–8 mm) or two (2–4 mm and 4–8 mm, each 50% by mass) standard size ranges. Cement paste content was highly decreased compared to that of normal concrete mixtures. The aggregate and cement contents of porous concrete are more efficiently expressed in terms of the aggregate to cement ratio by mass which was 5.7 in all the mixtures produced for this investigation. Two different types of aggregates (crushed basalt and river gravel), two binders (cement and silica fume), three different aggregate gradings and two levels of compaction were involved in the production.

In making the mixture design of porous concrete, the most critical requirement is to produce a cement paste of a standard consistency. The standard consistency of a cement paste for porous concrete, which can be defined as the cement particles being sufficiently distributed in the paste with a controlled workability, facilitates the formation of an evenly distributed cement paste phase throughout the specimen without the accumulation of access cement paste at any location especially at the bottom portion. Consistency of cement paste is dependent on various parameters such as the type of binder, water to cement ratio and the admixtures. Keeping the water to cement ratio constant at 0.30 for the strength requirements, the amounts and types of admixtures were adjusted according to the types of binders used. While the amount of superplasticizer is the most decisive parameter, the set retarder is also essential for maintaining the workability throughout the casting process that also involves a prolonged compaction. The summary of the compositional properties of the mixtures is given in Table 1.

The cement used was CEM I 52.5 Rapid hardening cement with a specific gravity of 3.13 g/cm^3 and Blaine fineness of 5330 cm^2/g. An undensified type of silica fume, with a SiO_2 content of 97%, was used for replacing cement in some mixtures. A polycarboxylic ether type of superplasticizer and a set retarder that provides a workability time of up to 3 h were used as admixtures. Crushed basalt with a specific gravity of 3.0 g/cm^3 and river gravel with a specific gravity of 2.60 g/cm^3 were sieved in size groups of 2–4 mm and 4–8 mm before use. Water to binder ratio was kept at 0.3 in all the mixtures.

Preparation of the porous concretes was done following a standardized procedure. If the mixture contains silica fume, cement and silica fume were first mixed in a separate mixer for mixing powders for five minutes prior to mixing with water. This was done to eliminate the agglomerates in the silica fume. Following the dry mixing, the dry binder content was mixed with water, superplasticizer and set retarder in a separate mixer for three minutes to make the cement paste. Consequently, the cement paste was mixed with the aggregates in a third and larger size rotary mixer for three minutes.

Compaction is essential in the casting of porous concrete while the type of compaction technique used is very effective on the ultimate porous concrete properties [11]. In this study, two compaction techniques were used, which were hand compaction using a steel cylinder and a special machine compaction technique using an impact hammer that displaces both in the vertical direction and vibrates at the same time while the hammer was also rotated,

Table 1
Compositional properties of the porous concrete mixtures.

Mixture code	PRC1	PRC2	PRC3	PRC4	PRC5	PRC6	PRC7	PRC8	PRC9
Aggregate composition									
Crushed basalt (2–4 mm) (gr)	–	2000	1000	–	–	2000	1000	–	–
Crushed basalt (4–8 mm) (gr)	2000	–	1000	–	2000	–	1000	2000	–
River gravel (4–8 mm) (gr)	–	–	–	2000	–	–	–	–	2000
Cement paste composition									
Cement (gr)	351	351	351	351	298	298	298	351	351
Silica fume (gr)		–	–	–	53	53	53	–	–
Water (gr)	105	105	105	105	105	105	105	105	105
Superplasticizer (gr)	0.97	0.97	0.97	0.97	1.30	1.30	1.30	1.00	1.00
Set retarder (gr)	1.20	1.20	1.20	1.20	1.20	1.20	1.20	–	–
Cement paste code	cp1	cp1	cp1	cp1	cp2	cp2	cp2	cp3	cp3
Compaction	High	High	High	High	High	High	High	Low	Low

Table 2
Compositional properties of the normal concrete mixture.

NC1 composition	Amounts (kg)
CEM I 42.5N	3.10
0.125–0.250 mm sand	1.32
0.250–0.500 mm sand	2.44
0.500–1 mm sand	2.82
1–2 mm sand	2.82
2–4 mm sand	3.76
4–8 mm river gravel	5.64
Water	1.75
Superplasticizer	1.8%

Table 3
Properties of the steel used in the impactor.

Material properties	Steel
Elasticity modulus, E (GPa)	200
Density, ρ (g/cm^3)	7.9
Poisson's ratio, v	0.28
Shear modulus, G (GPa)	78.1
Bulk modulus, K (GPa)	151.5
Longitudinal wave velocity, C_l (m/s)	5689

which were expressed as low and high in Table 1, respectively. During the trial productions, the amount and method of compaction were progressively modified as to ensure that the samples nearly reach the maximum compaction that was possible in practice. During the compaction, also because the hammer end was covered with a layer of a soft type of rubber, the aggregates were displaced with the aid of friction into an arrangement that drastically modified the aggregate orientations and packing. Compaction was applied to every 2.5 cm layer and every layer was compacted five times. Before adding the next layer, the top of the last layer was roughened using a fork to provide a better interlock. During each blow, the mold was rotated in the clockwise direction while the hammer was rotated in the counter-clockwise direction to be able to better move the aggregates into the available space. In porous concrete applications where permeability is required, pore connectivity is essential, compaction is restricted due to the fact that it reduces pore connectivity. In this investigation, because applications related to safety purposes are aimed, pore connectivity was not required.

Cylindrical specimens that were 83 mm in diameter, 170 mm in height were cast, where two impact test samples were drilled from each specimen. Because the mixing and compacting procedures are lengthy, the use of a set retarder was essential in order to maintain the required level of workability of the cement paste.

A moderate strength normal concrete was also produced in order to compare the results obtained for porous concrete with a normal concrete. The mixture properties of the normal concrete mixture (NC1) produced is presented in Table 2.

Both porous and normal concrete specimens were wrapped with plastic and aluminum foils and kept at 20 °C at the laboratory conditions until their testing dates of 28 days. Core samples of 60 mm diameter were then drilled from the specimens and cut at the fixed height of 70 mm to be tested at the drop weight impact test. In the impact tests, five samples were tested for each porous concrete mixture while seven samples were tested for the normal concrete mixture.

2.2. Test set-up and instrumentation

Instrumented drop-weight impact tests were performed using LDV as the monitoring technique. In the LDV experiments a Polytec OFV 505 laser head and OFV 5000 controller (with a sampling frequency capacity of 2 GHz) having a VD 06 velocity decoder were used. Measurements with sampling frequencies of 500 kHz and 400 kHz were taken by using a LeCroy Wavesurfer 432 digital oscilloscope. Trigger threshold was set at the velocity of 3 m/s where the measurement block length and trigger delay time were set at 2 s and −1 s, respectively.

A steel impactor was used at the drop weight tests. Steel is selected as the impacting material due to its high dynamic impedance. Material properties of the impactor used are important because they are directly involved in impact stress calculations. Using the Youngs modulus and the Poissons ratio provided by the manufacturer, the shear and bulk moduli and consequently the longitudinal wave velocity of the steel used in the impactor was calculated adopting Eq. (1) [20]. The material properties of the steel used is presented in Table 3.

$$C_i = \sqrt{\left[\frac{K + \frac{4}{3G}}{\rho}\right]} \tag{1}$$

In the experiments, the specimen was placed vertically on a steel base structure, which also functions as a wave sink. Impactor was dropped from approximately 1.2 m striking the target specimens at velocities ranging between 4.0 and 4.7 m/s. A steel impactor with a diameter of 110 mm and a height of 220 mm was used. After the collision, the impactor was stopped by a protective chamber to protect the target, which had already failed due to the stress waves, from being crushed by the self-weight of the impactor.

Impactor diameter (110 mm) was selected to be larger than the diameter of the target (60 mm) to be able to take velocity measurements at the interface. Meanwhile, the point where the laser beam hits the impactor was adjusted to be as close as possible to the specimen perimeter. The horizontal laser beam sent from the laser head was reflected from a 45° mirror so that it was then directed

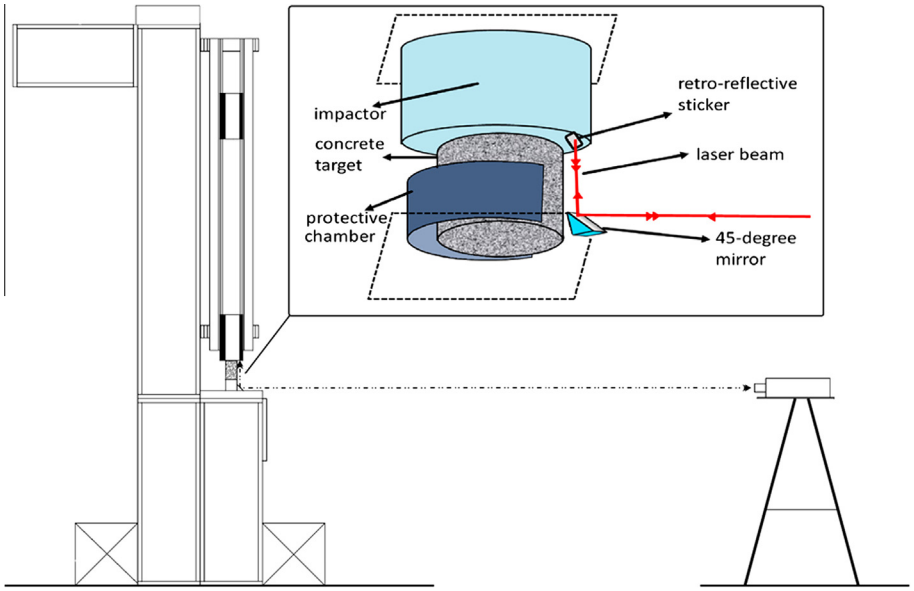

Fig. 1. Schematic view of the testing system.

upwards in the vertical direction. The reflected vertical beam hitting the retro-reflective sticker attached to the bottom surface of the impactor rim was reflected again and followed the same path back to the laser head. The particle velocity time histories of the interface between the target and the impactor were captured and afterwards analyzed to determine the impact stress applied on the target. The testing system and a detailed view of how the laser beam is reflected are schematically presented in Fig. 1.

3. Measurement and analysis techniques

The main features of the method used are presented in Fig. 2. At the drop weight impact tests, the particle velocity histories of the interface (between the impactor and the concrete target) were captured using LDV. The data was analyzed using a special application of the reverberation technique where the dynamic impedance of the impactor was required as input. As a result of the analyses, the impact strengths of the target concrete samples were obtained [19].

At the drop weight test, at the moment of collision when the impactor hits the concrete target, two compression shock waves are generated at the impact plane which constitutes the interface between the impactor and the target. The compression stress wave traveling in the specimen is presented in Fig. 3 using a Lagrangian diagram where x is the spatial coordinate and t is time. After the collision, one wave propagates down into the specimen and the other propagates up into the impactor. The compressive pulse that propagates down the specimen arrives at the bottom interface between the bottom surface of the specimen and the steel base of the test set-up. A transmitted pulse is sent into the steel base while a reflected compressive pulse is sent back into the specimen with a magnified amplitude because the dynamic impedance (Z) of the steel base is greater than that of the target concrete specimen. $Z = \pm\rho C$ where ρ, C are the density and the related wave velocity of the material, respectively. When the compressive pulse reflected from the bottom interface propagates upward and reaches the top interface, it again reflects back into the specimen as a magnified compressive pulse. Several of these reverberations occur within the specimen increasing the magnitude of the compressive pulse at each reflection [8,21]. Because the target is very short compared to the impactor and the steel base structure of the test set-up, the

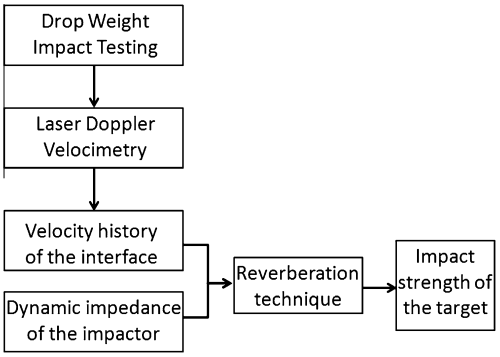

Fig. 2. The main features of the method used.

shock wave that travels in the target makes several reflections before the waves that travel in the impactor and the set-up reflect back [21].

3.1. Impedance mismatch method and reverberation technique

In determining the response of a material to a shock wave, it is widely accepted to approximate compression paths using Hugoniot curves. A shock wave causes the material to jump between the initial state and the final shocked state points on the Hugoniot. [8,22,23]. In planar impact studies, the pressure versus particle velocity relationship is analyzed using a technique based on intersecting the Hugoniots of the impactor and the target, which is called the impedance mismatch method. At the intersection of the two Hugoniots, the situation of equal pressures and particle velocities due to the principle of continuity at the interface is valid [23].

When there are two interfaces present in the experimental system instead of one interface, as in the experimental configuration in this study, the impedance mismatch analysis is slightly more intricate. Similar configurations, where the sample is impacted between two higher dynamic impedance materials, have been investigated by researchers [23–25]. Because the reflected wave keeps the sign of the incident wave when it reflects from a higher dynamic impedance material, each reflection successively again in-

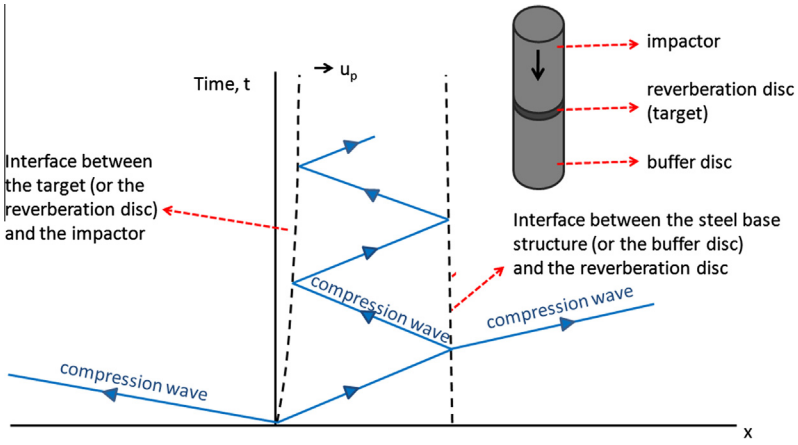

Fig. 3. Lagrangian diagram for a low impedance material impacted between two high impedance media.

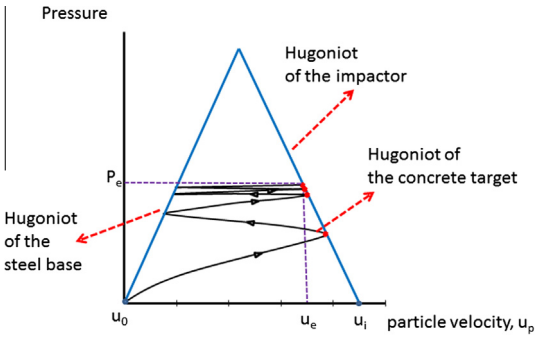

Fig. 4. Impedance mismatch graph for a concrete target impacted between two metals.

creases the amplitude of the compression wave in the target also like in the testing configuration for porous concrete. In the reverberation studies presented in literature, the target is a linear elastic material with a dynamic strength that is sufficient to withstand the maximum stress that can be applied by that test configuration at that impact velocity. Therefore, the stress continues to increase until that maximum value is reached which is also considered to be an equilibrium state in pressure [23–25]. This method can also be applied when testing nonlinear materials with dynamic strengths that cannot withstand that maximum stress, as in the tests conducted in this research where the targets are either porous concrete or normal concrete. In this case, unlike the reverberation process happening when a strong linear elastic material is tested, the reverberation situation continues until the stress within the concrete specimen reaches a value that generates substantial inelastic strains in the material beyond which further wave propagation within the specimen can be neglected. Therefore, the amplitude of the subsequent wave fronts is very small [26]. This situation can be seen in the impedance mismatch figure illustrated in Fig. 4 where the two main blue lines correspond to the Hugoniots of the steel impactor and the steel base structure of the set-up. The lines that travel between those two Hugoniots represent the behavior of the target concrete that is being compacted. The red spots on the Hugoniot of the impactor are the points where the Hugoniots of the impactor and the target material intersect and therefore where the stress and particle velocities of the target and the impactor are equal. In the figure, these points eventually come to an equilibrium level that corresponds to a stress value of P_e. The velocity values of those red points are the particle velocity values measured through LDV during the test.

As seen in Fig. 4, because the particle velocity is measured on the impactor, it also reaches an approximately constant value when the pressure reaches equilibrium. This velocity value is named equilibrium velocity (u_e) because it corresponds to the particle velocity value when the stress reaches equilibrium.

In Fig. 5, a typical Laser Doppler velocimetry signal from a drop weight impact experiment of a PRC1 porous concrete sample impacted by a steel impactor is presented. In the figure, the first part that seems horizontal corresponds to the free fall of the impactor with a slope of gravitational acceleration minus the friction. After the free fall part, there is the collision followed by wave reverberations. A very clear plateau was observed in both porous and normal concrete samples. The last part of the plateau in the figure corresponds to the part where the impactor hits the protective chamber which has no significance in the analysis. The measurements were done at the frequency of 400 kHz (later filtered with a cutoff frequency of 20 kHz) . The strain rate measured on the samples using a high speed camera at a frame rate of 10,000 frames/s was found to be 68 s^{-1} on average.

3.2. Analysis of particle velocity histories

To be able to obtain the stress from the measurements of the particle velocity, conservation of momentum law, which is also the principle behind the impedance mismatch method, was used. In the conservation equation, the pressure P applied to the target material is equal to the momentum transferred by the impactor to the target per unit time as given in the following equation.

$$P - P_0 = \rho_0 C(u_i - u_e) \tag{2}$$

where P, P_0, ρ_0, C, u_i and u_e are the shock pressure, initial pressure, initial density, wave velocity, impact velocity and the equilibrium velocity, respectively. In solids, the shock pressure P is much greater than the initial pressure P_0 (the ambient atmospheric pressure) which is usually neglected [23,27]. As the equilibrium is reached, the stationary target concrete with zero velocity reaches the equilibrium velocity (u_e). Meanwhile, the impactor with the impact velocity (u_i) decelerates to the same velocity. Therefore, the analyses were made by first obtaining the impact and equilibrium velocity values from the particle velocity history plots as in Fig. 5 and then by calculating the stress using impedance mismatch. Because the concretes that were tested at the experiments failed and reached the limits of their dynamic strengths, the stresses that were calculated are the dynamic strengths of the specimens tested.

In these analyses, the stress is calculated using the dynamic impedance properties of only the impactor and therefore the prop-

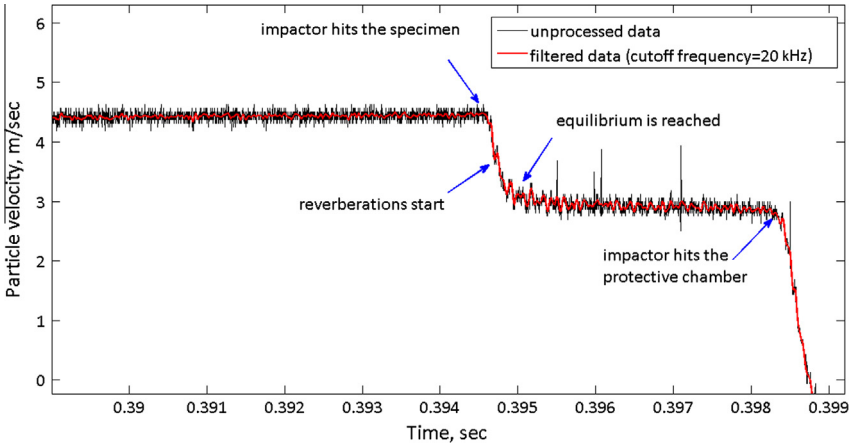

Fig. 5. Doppler laser velocimetry signal from a drop weight impact test of porous concrete.

erties of the target are not needed in the calculations. Meanwhile, taking the measurements on a highly stiff impactor with a large height allows to capture an average response and rules out the local variations in the shock and particle velocities in the concrete. Therefore, the impedance variations in heterogeneous materials like concrete that drastically affect the local measurements are not influential on the results [28].

3.3. Dynamic increase factor calculations

Dynamic increase factor (DIF), which is the ratio of dynamic strength to static strength, is widely used as an indication of the effect of strain rate, $\dot{\varepsilon}$, on the strength of cementitious materials. The static compression tests were conducted using a closed loop deformation controlled test set-up at the loading rate of 1 μm/s. Experimental and empirical (using the formula of Comité Euro-International du Béton, CEB) DIF values were also calculated for each mixture to compare the increase in strength under dynamic loading of different porous concretes with those of conventional concretes with the same static strengths. This comparison gives the opportunity to see how predictable the dynamic strengths of various porous concretes are using the widely used DIF equation of CEB. The CEB relation between DIF and the strain-rate (Eq. (3)) is as follows, at which a bilinear relation between DIF and log $\dot{\varepsilon}$ with a breakpoint at the strain rate of 30 s^{-1} is defined [29].

$$\mathrm{DIF} = \frac{F_{cd}}{f_{cs}} = \left[\frac{\dot{\varepsilon}}{\dot{\varepsilon}_s}\right]^{1.026\alpha_s} \quad (\text{for } \dot{\varepsilon} \le 30\ \mathrm{sec}^{-1}) \quad \text{and} \quad \mathrm{DIF} = \gamma_S \left[\frac{\dot{\varepsilon}}{\dot{\varepsilon}_s}\right]^{1/3} \quad (\text{for } \dot{\varepsilon} \geqslant 30\ \mathrm{sec}^{-1}) \tag{3}$$

where f_{cd} and f_{cs} are the uniaxial dynamic and quasi-static compressive strengths, respectively. In the equations, $\dot{\varepsilon}_S = 30 \times 10^{-6}\ s^{-1}$, $\gamma_S = 10^{(6.156\alpha s - 2.0)}$, $\alpha_s = 1/(5 + 9f_{cs}/f_{co})$, $f_{co} = 10$ MPa.

3.4. Porosity measurements

The porosity values of the samples were obtained through computed tomography using a Phoenix Nanotom CT scanner. During the computed tomography application, two dimensional X-ray images are taken while rotating the specimen 360° around the axis of rotation. The two dimensional images are reconstructed to generate a three-dimensional image enabling the analysis of the specimen at any section taken both vertically and horizontally at any angle. In the CT image, different materials are indicated by different shades of gray due to the variations in the density. The analysis to determine the porosity of the specimen is therefore particularly efficient due to the great difference in the densities of the solid phases and air. The image is then converted into a binary image (as seen in Fig. 6) while the ratio of the pixels corresponding to the air phase to the whole sample is taken as the porosity.

3.5. Sieve analysis of post-failure fragments

After the impact test, the samples were also analyzed at their post-failure state by sieving the remaining fragments of the samples. The presence of the protective chamber in the experimental set-up, that stops the impactor after it displaces down about 2.5 cm following the collision, prevented the impactor from crushing the post-failure fragments with its self-weight. Various definitions of fragment size are present [30]. When grains are not close to spherical, the size measurements are usually practically expressed in terms of the diameters of equivalent spheres i.e. the sieve results are reduced to the nominal diameter of a sphere.

4. Results and discussion

The impact strengths of nine different types of porous concretes and one mixture of normal concrete were investigated. The effects of different compositional factors on the properties of porous concrete were evaluated. The fracture pattern observation using high speed photography and post failure sieve analysis were also performed on the samples.

4.1. Impact test results of different types of porous concretes and normal concrete

The results of tests applied on porous concretes are presented in Table 4. If the results are evaluated in terms of aggregate properties, it can generally be said that aggregate properties such as grading, size, shape, texture and strength have a major influence on the dynamic strength of porous concrete due to the coarse aggregates being very dominant in the formation of the final material structure.

According to the results, it was seen that as two sizes of aggregates (2–4 and 4–8 mm) were used instead of using single sized aggregates, the dynamic strengths of porous concretes as well as their static strengths increased. Among all the mixtures tested, PRC3 and PRC7, which included aggregates of two sizes, offered the highest dynamic strengths which were 85.99 MPa and 84.37 MPa, respectively. As their porosity values (18.77% and

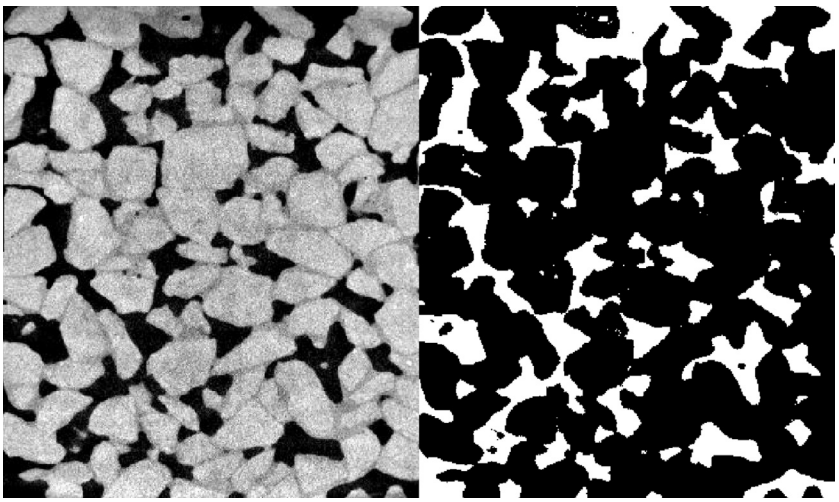

Fig. 6. Determination of porosity using computed tomography.

Table 4
Results of the impact tests conducted on different types of porous concretes.

Mixture code	Impact velocity (m/s)	Equilibrium velocity (m/s)	Dynamic strength (MPa)	Porosity (%)	Average dynamic strength (MPa)	Average static compressive strength (MPa)
PRC1	4.46	2.93	68.76	21.78	66.52	34.78
PRC1	4.48	3.01	66.07			
PRC1	4.48	2.98	67.41			
PRC1	4.49	3.00	66.97			
PRC1	4.47	3.06	63.37			
PRC2	4.34	2.71	73.30	20.33	76.78	41.89
PRC2	4.50	2.73	79.59			
PRC2	4.52	2.83	75.86			
PRC2	4.47	2.78	76.09			
PRC2	4.53	2.77	79.05			
PRC3	4.31	2.42	84.81	18.77	85.99	50.49
PRC3	4.51	2.71	80.72			
PRC3	4.49	2.68	81.21			
PRC3	4.49	2.35	96.40			
PRC3	4.42	2.49	86.79			
PRC4	4.50	3.16	60.63	17.93	56.22	29.64
PRC4	4.42	3.22	53.84			
PRC4	4.46	3.12	60.36			
PRC4	4.47	3.40	48.27			
PRC4	4.49	3.20	58.02			
PRC5	4.49	3.24	55.91	21.98	53.09	31.60
PRC5	4.49	3.17	59.64			
PRC5	4.49	3.30	53.75			
PRC5	4.45	3.43	45.66			
PRC5	4.41	3.29	50.47			
PRC6	4.44	2.67	79.41	20.12	79.69	44.81
PRC6	4.43	2.62	81.44			
PRC6	4.48	2.63	83.28			
PRC6	4.54	2.88	74.63			
PRC7	4.48	2.79	75.86	18.63	84.37	48.80
PRC7	4.47	2.47	90.25			
PRC7	4.46	2.73	77.93			
PRC7	4.49	2.40	93.89			
PRC7	4.48	2.62	83.91			
PRC8	4.46	3.90	25.17	24.75	26.26	15.94
PRC8	4.34	3.72	27.86			
PRC8	4.30	3.67	28.31			
PRC8	4.34	3.73	27.42			
PRC8	4.33	3.84	22.02			
PRC9	4.43	3.95	21.57	–	21.84	13.09
PRC9	4.40	3.88	23.37			
PRC9	4.47	4.02	20.22			
PRC9	4.49	3.94	24.72			
PRC9	4.55	4.12	19.33			

18.64%, respectively) are also compared with the porosities of the other mixtures, it is seen that the dynamic strength of porous concretes increases due to the fact that aggregate grading is coupled with the total porosity which is the main factor that affects the strength.

When mixtures having single sized aggregates are compared, it is seen that as the aggregate size decreases the dynamic strength of the mixtures increases. The two mixtures PRC1 and PRC2 having single-sized aggregates and the same mixture compositions except their aggregate sizes (which were 4–8 mm and 2–4 mm, respectively) had dynamic strengths of 66.52 MPa and 76.78 MPa, respectively. The same trend was true for PRC5 and PRC6 (with 4–8 mm and 2–4 mm aggregates, respectively) that had the dynamic strengths of 53.09 MPa and 79.69 MPa, respectively. If the porosity values for the mixtures are compared, it is seen that there are very slight differences between the porosities of all those mixtures. While the total percentages of the intentional pores present in single-sized aggregate mixtures are already expected to be similar irrespective of the aggregate size, the increase in dynamic strengths can be explained by the increase in contact or bonding areas as the aggregate size decreases.

As mixtures PRC1 and PRC4 are compared, the difference between their dynamic strengths can be explained by a combination of several factors. The two mixtures have the same properties in terms of their mixture compositions except that river gravel was used in PRC4 instead of crushed basalt. River gravel tends to have a more equi-dimensional and rounded shape compared to crushed basalt. Crushed basalt also have more texture. Due to these differences in shape and texture, the porosity of PRC4 (17.93%) was considerably lower than that of PRC1 (21.78%). It is even the lowest among all the mixtures. However, increased aggregate texture and angularity contribute to porous concrete strength due to enhanced mechanical interlock, increased total surface area available for the adherence of the cement paste and increased contact points. Basalt being an aggregate with a higher strength compared to most of the different types of aggregates present the river gravel batch is another factor. As a result of all the factors present, the dynamic strength of PRC4 (56.22 MPa) was lower than the dynamic strength of PRC1 (66.52 MPa).

While aggregate properties were very influential, the effect of changing the binder composition of cement paste did not have a very significant effect on the dynamic strengths. Replacing 15% of cement paste by silica fume did not enhance and even slightly decreased the dynamic strengths of the mixtures. Meanwhile, the effect of the compactive effort on the impact strengths of porous concrete can be seen when PRC8 and PRC9 are compared with the other mixtures. While an intensive compaction was applied to the other mixtures, PRC8 and PRC9 were hand compacted by using a steel cylinder. The drastic decrease in the strength values of these two mixtures can therefore be attributed to poor particle packing and high porosity. While no set retarder was used in mixtures PRC8 and PRC9, due to hand compaction not being as long during as the machine compaction, this could have also had an effect on the decreased dynamic strength values.

Drop weight impact tests were also applied on a moderate strength normal concrete to compare its results with the results of porous concretes. As in the impact tests performed on porous concrete samples, in normal concrete testing the plateau was very clearly observed and the samples completely failed during the test. The results of the tests are presented in Table 5.

The average static strength of the samples from the same concrete mixture was 26.44 MPa which corresponds to a dynamic increase factor (DIF) of 2.19. At the strain rate of 68 s^{-1}, the DIF value is empirically calculated to be 2.15 according to Eq. (3) which is very close to the value of 2.19 that was obtained experimentally for normal concrete. The DIF value obtained for normal concrete is also consistent with the widely referenced review on the effect of strain rate conducted by Bischoff and Perry [31].

Similar to normal concretes, porous concretes are strain rate dependent materials due to the presence of the cementitious phases. The DIF values obtained from the experiments compared to the DIF values calculated using the CEB equations that are normally valid for conventional concretes are presented in Table 6. The experimental DIF values of the porous concrete mixtures that have significantly high static strengths, to be considered as porous concretes, are highly consistent with the DIF values calculated using CEB equations except for PRC5. The contradicting DIF values obtained for mixtures PRC8 and PRC9, that have not been sufficiently compacted, show that the CEB equations are not valid for low strength, insufficiently compacted porous concretes with a higher porosity. However, they give considerably accurate results for well compacted high strength porous concrete mixtures for the strain rate of the performed drop weight tests which was 68 s^{-1}.

4.2. Fracture patterns of porous concrete loaded under drop weight loading

In the high speed camera measurements, be able to visualize the whole sample, the photographs that are presented below were taken at 6134 frames/s. In Fig. 7, the dotted vertical lines indicate the frequency of the photographs captured. Four representative photographs were selected to be presented in Fig. 8. The timings of the photographs that were selected were indicated in Fig. 7 as A–D.

The photos presented in Fig. 8 were taken from a typical drop weight impact test performed on a PRC1 sample. In the photographs, it can progressively be seen that under impact loading cracks propagate and coalesce to form small particles due to the stress wave.

Table 5
Results of the impact tests conducted on normal concrete.

Test no.	Impact velocity (m/s)	Equilibrium velocity (m/s)	Dynamic strength (from Eq. (2)) (MPa)
1	4.29	1.34	60.22
2	4.36	1.29	57.98
3	4.08	1.25	56.18
4	4.38	1.39	62.47
5	4.34	1.23	55.28
6	4.29	1.27	57.08
7	4.35	1.26	56.63
Average dynamic strength (MPa)			57.97

Table 6
Experimental and calculated DIF values for porous and normal concretes.

Mixture code	PRC1	PRC2	PRC3	PRC4	PRC5	PRC6	PRC7	PRC8	PRC9	NC
Static comp. strength	34.78	41.89	50.49	29.64	31.60	44.81	48.80	15.94	13.09	26.44
Dynamic comp. strength	66.52	76.78	85.99	56.22	53.09	79.69	84.37	26.26	21.84	57.97
DIF (experimental)	1.91	1.83	1.70	1.90	1.68	1.78	1.73	1.60	1.73	2.19
DIF (calculated using Eq. (3))	1.94	1.83	1.74	2.01	2.00	1.80	1.76	2.73	3.06	2.15

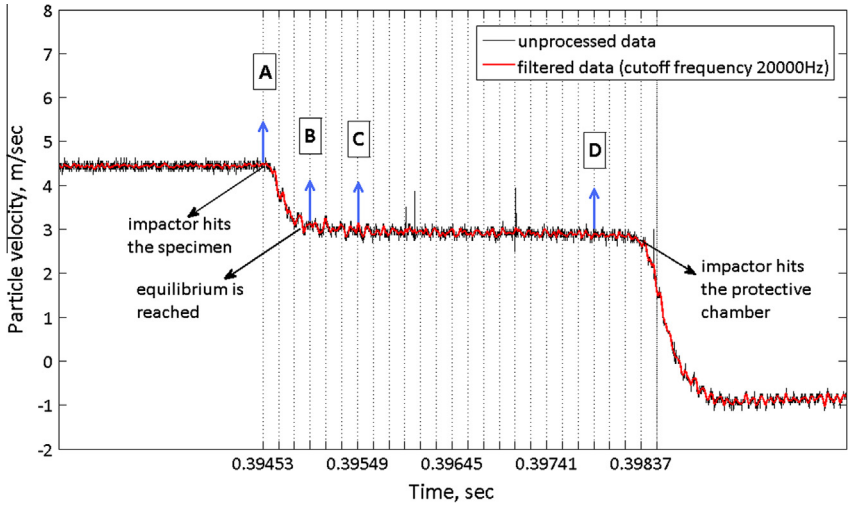

Fig. 7. Particle velocity history plot indicating the timing of the photographs.

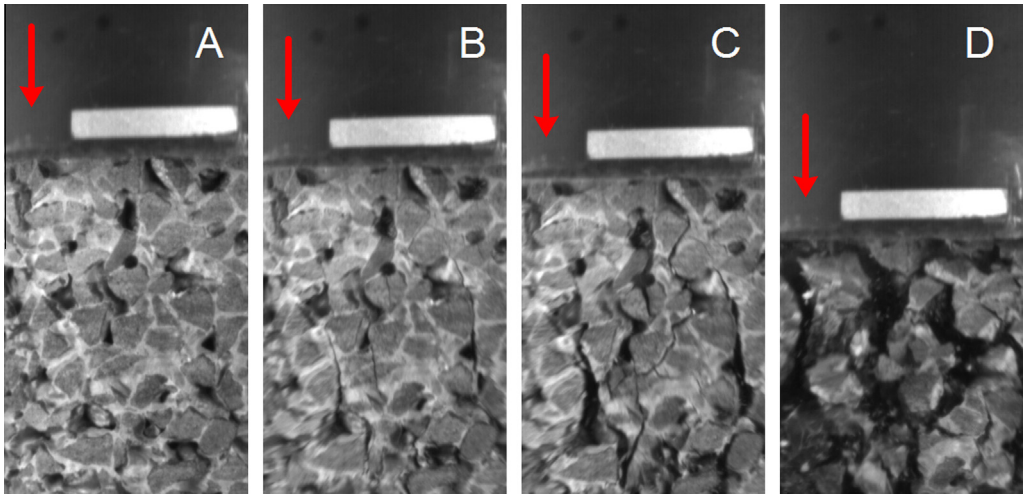

Fig. 8. Photographs demonstrating fracture patterns.

In porous concrete, similar to normal concrete microcracks are expected to predominantly initiate from the interface and subsequently propagate into the bulk cement paste. The crack patterns that are observed in Fig. 8 are also similar to those of normal concretes in the sense that tensile cracks parallel to the axis of loading and the subsequent shear cones underneath the aggregates can be observed [32]. However, differently in porous concretes, the crack patterns are also guided by the porous structure. It should also be noted that the fracture patterns observed during the test and the fragments that are examined after failure demonstrate that cracks are not solely located in the cement paste, but are also sometimes forced to propagate through the aggregates.

4.3. Sieve analysis results of fragments

The results of the sieve analysis are presented in Table 7. Fragments of four different specimens (from each mixture) that had gone through drop weight impact testing were sieved and the average of those four results was taken for each sieve opening size. During the tests, it was observed that triaxially stressed cones at the end parts of the specimens were formed and remained intact due to the boundary friction between the loading platen and the specimen. The percentage by mass of the two cones that remain were about 20% in each sample for the sizes of samples that were tested in this study (60 mm diameter–70 mm height). The sieving

Table 7
Sieve analysis results of the fragments for different mixtures.

Mixture code	PRC1	PRC2	PRC3	PRC4	PRC5	PRC6	PRC7	PRC9
Aggregate size (mm)	4–8	2–4	50% 2–4, 50% 4–8	4–8	4–8	2–4	50% 2–4, 50% 4–8	4–8
Sieve size (mm)				% Aggregate retained				
32	0.21	0.33	0.27	0.18	0.20	0.36	0.21	0.20
16	0.07	0.07	0.13	0.12	0.08	0.08	0.17	0.07
8	0.25	0.12	0.18	0.25	0.23	0.09	0.21	0.25
4	0.37	0.19	0.23	0.30	0.39	0.21	0.23	0.38
<4	0.10	0.28	0.19	0.15	0.10	0.27	0.18	0.10
Cumulative < 16	0.72	0.59	0.60	0.70	0.72	0.57	0.62	0.73

results of PRC9, which was one of the weakest mixtures fracturing completely into small size fragments except the mentioned triaxially stressed cones that remained intact, are an indication of those conical parts constituting approximately 20% of the mass of a sample as seen in Table 7.

During the sieve analysis, it was also observed that the fragments that were formed were slim in shape having one dimension very different from the others due to the fragment patterns that can also be observed in Fig. 8 where the vertical tensile cracks cause the formation of slender fragments. If the fragments are sized in terms of the diameters of equivalent spheres, taking the area as reference, the diameter of the circle with the same area as the maximum projected profile of a fragment is taken as the fragment size.

If this is applied, as an example, to one representative large-size fragment shown in Fig. 9, it is found that a fragment that has a length of 22.3 mm (remaining on the 16 mm sieve) has a corresponding equivalent diameter of 12.6 mm. It is not possible to evaluate each fragment through such a calculation, but when quantifying fragmentation, the evaluation of the sieve analysis should actually be done also taking the shapes of the fragments into concern.

According to the results presented in Table 7, it can be said that the percentage of the fragments larger than 32 mm was mostly caused by the confined cones formed at the ends of the samples. If the percentages of the fragments that are smaller than 16 mm are taken as reference, it is seen that PRC1, PRC4 and PRC5 showed a good performance in terms of fracturing into small fragments while having sufficient strength. If PRC6 and PRC7 (or PRC2 and PRC3) are compared it is seen that even though PRC7 had a lower porosity and higher dynamic strength than PRC6 due to containing aggregates at two sizes, it fractured into smaller fragments. The same can also be said for mixtures PRC2 and PRC3. Meanwile, PRC9, which had the smallest sized fragments, had a very low static strength value. As the results in the table are evaluated further, it can be seen that the distributions of fragment sizes smaller than 16 mm also show variations in the different mixtures. In mixtures PRC2 and PRC6, fragments smaller than 4 mm are consistently more than those of other mixtures such as PRC1 and PRC5 while the sizes of fragments of the latter mixtures were mostly concentrated at the range of 4–8 mm.

According to the results, the fragmentation performance of the different mixtures are mostly affected by the aggregate size. The common feature of mixtures PRC1, PRC4 and PRC5 that gave the least amount of fragments larger than 16 mm was the grading of their aggregates (4–8 mm), which was the coarsest grading among all the mixtures. The same factor is also apparent when PRC6 and PRC7 (or PRC2 and PRC3) are compared. Due to their contents of 4–8 mm aggregates, PRC3 and PRC7, which actually have lower porosity and higher strength values than PRC 2 and PRC6, gave equal and even slightly less amount of fragments larger than 16 mm. This can be explained by the fact that when the aggregate grading is finer, the amount of contact surface (per aggregate volume) between the neighboring aggregates is higher. Therefore, each aggregate is bonded more strongly to its neighbors. On the other hand, when the finer portion of the fragment size distribution is of concern, the amount of finer fragments (<4 mm) are higher in mixtures containing 2–4 mm aggregates compared to the mixtures with 4–8 mm aggregates which is expected due to the minimum sizes of aggregate particles that are present. However, the percentage of larger size fragments (> 16 mm) being higher, which is the main concern in terms of safety applications, make the fragmentation performance of those mixtures less favorable. In the process of selecting a mixture to be used in safety structures, the evaluation should be done according to the service loads and the amplitude of impact stress the concrete is expected to be exposed to in that specific application. Therefore, mixtures PRC1, PRC4 and PRC5 (having sufficient static strengths and small-size fragments) and PRC2, PRC3, PRC6 and PRC7 (having higher static strengths, but slightly larger fragment sizes) should be evaluated through optimization in terms of their static strengths and fragment sizes according to the design requirements.

Fig. 9. Post-failure fragment and its maximum projected profile.

5. Conclusions

In the research presented in this study, different types of porous concretes were produced and subjected to drop weight impact tests. Porous concretes that fractured into small fragments under impact loading, while having sufficient static strength, were produced by modifying various compositional properties and the production technique. According to the results obtained, the aggregate properties and compactive effort are main factors that affect the dynamic performance of porous concrete.

- When mixtures containing different shapes and types of aggregates are compared, it is seen that increased texture and angularity contribute to porous concrete strength due to enhanced mechanical interlock, increased total surface area available for the adherence of cement paste and increased contact points. The strength of the aggregates used also has an influence on the strength of the final material.
- When two sizes of aggregates were used instead of using single sized aggregates, the dynamic strengths of porous concretes as well as their static strengths increased. This is due to the aggregates having different sizes showing a more efficient packing because of smaller particles being better located into the voids between larger. For mixtures having single sized aggregates, as the size of the aggregates decreases, dynamic strength is also enhanced due to the increase in contact or bonding areas.
- Compaction is a factor that has an important effect on the strength properties because it directly affects the porosity. As intensive compaction enhances the strength properties, insufficient compaction of some of the mixtures tested caused a drastic decrease in the both the static and the dynamic strengths.
- While aggregate properties drastically affect the strength properties, changing the cement paste composition did not have a very significant effect on the dynamic strengths of the samples.
- By comparing the static and dynamic strength results of different porous concretes as well as a moderate strength normal concrete, it is concluded that porous concretes are strain-rate-

dependent materials like normal concretes. Therefore with the increase in strain rate, there is an increase in the dynamic strength values obtained. The CEB equations used for correlating the DIF and the strain-rate in normal concretes give considerably accurate results for well compacted high strength porous concrete mixtures while they are not valid for low strength, insufficiently compacted porous concretes.

– The fracture patterns of porous concretes were observed using high speed photography in order to visualize how cracks propagate and coalesce to form small particles due to stress wave propagation. In the photographs, it was observed that the crack patterns were influenced by the geometry of the void structure in porous concrete and by the presence of the thin cement paste bridges that bond the coarse aggregates. Post-failure sieving of the fragments of the specimens was also performed in order to quantify their sizes. According to the results, it can be said that for some of the porous concrete mixtures, the fragments were sufficiently small to meet the design objectives. The mixture of porous concrete to be used in a particular safety structure should be selected according to optimization in terms of static strength and fragment size depending on the design requirements.

Acknowledgements

This project was funded by the Netherlands Ministry of Defence. The authors would also like to acknowledge the Engineering Dynamics Section of the Faculty of Mechanical, Materials and Maritime Engineering at Delft University of Technology for providing the Doppler laser velocimetry equipment. The authors would also like to thank Ger Nagtegaal and Gerard Timmers for their contributions to establishing the test set-up.

References

[1] Yang J, Jiang G. Experimental study on properties of pervious concrete. Cem Concr Res 2003;33(3):381–6.
[2] Chindaprasirt P, Hatanaka S, Chareerat T, Mishima N, Yuasa Y. Cement paste characteristics and porous concrete properties. Constr Build Mater 2008;22(5):894–901.
[3] Ghafoori N, Dutta S. Development of no-fines concrete pavement applications. J Transport Eng 1995;121(3):283–8.
[4] Marolf A, Neithalath N, Sell E, Wegner K, Weiss J, Olek J. Influence of aggregate size and gradation on the acoustic absorption of enhanced porosity concrete. ACI Mater J 2004;101(1):82–91.
[5] Lankford J, Blanchard CR. Fragmentation of brittle materials at high rates of loading. J Mater Sci 1991;26(11):3067–72.
[6] Grote DL, Park SW, Zhou M. Dynamic behavior of concrete at high strain rates and pressures: I. Experimental characterization. Int J Impact Eng 2001;25(9):869–86.
[7] Zhang MH, Shim VPW, Lu G, Chew CW. Resistance of high-strength concrete to projectile impact. Int J Impact Eng 2005;31(7):825–41.
[8] Crouch LK, Pitt J, Hewitt R. Aggregate effects on pervious Portland cement concrete static modulus of elasticity. J Mater Civil Eng 2007;19(7):561–8.
[9] Erdogan ST, Fowler DW. Determination of aggregate shape properties using X-ray tomographic methods and the effect of shape on concrete rheology. Austin, Texas: International Center for Aggregates Research; 2005.
[10] ASTM. Significance of tests and properties of concrete and concrete-making. In: Paul Klieger P, Lamond JF, editors. ASTM Publication; 1994.
[11] Lian C, Zhuge Y. Optimum mix design of enhanced permeable concrete – an experimental investigation. Constr Build Mater 2010;24(12):2664–71.
[12] Kevern JT, Schaefer VR, Wang K. Evaluation of pervious concrete workability using gyratory compaction. J Mater Civil Eng 2009;21(12):764–70.
[13] Yeh Y, Cummins HZ. Localized fluid flow measurements with an He–Ne laser spectrometer. Appl Phys Lett 1964;4(1):176–8.
[14] Wu E, Sheen HJ, Chen YC, Chang LC. Penetration force measurement of thin plates by Laser Doppler anemometry. Experiment Mech 1994;34(1):93–9.
[15] Birch RS, Jones N. Measurement of impact loads using a Laser Doppler velocimeter. In: Proceedings of the institution of mechanical engineers. Part C. Mechanical engineering science. Sage Publications; 1990. p. 1–8.
[16] Hodgkinson JM, Vlachos NS, Whitelaw JH, Williams JG. Drop-weight impact tests with the use of laser-Doppler velocimetry. In: Proceedings of the royal society of London. Series A, mathematical and physical sciences. Great Britain: The Royal Society; 1982. p. 133–44.
[17] Ong KCG, Basheerkhan M, Paramasivam P. Resistance of fibre concrete slabs to low velocity projectile impact. Cement Concr Compos 1999;21(5–6):391–401.
[18] Habel K, Gauvreau P. Response of ultra-high performance fiber reinforced concrete (UHPFRC) to impact and static loading. Cement Concr Compos 2008;30(10):938–46.
[19] Agar Ozbek AS, Weerheijm J, Schlangen E, van Breugel K. Drop weight impact strength measurement method for porous concrete using Laser Doppler velocimetry. J Mater Civil Eng 2012;24(10):1328–36.
[20] Kipp ME, Grady DE. Shock compression and release in high-strength ceramics. Sandia National Laboratory Report, SAND 89-1461; 1989.
[21] Drumheller DS. Introduction to wave propagation in nonlinear fluids and solids. Cambridge: Cambridge University Press; 1998.
[22] Asay JR, Shahinpoor M. High-pressure shock compression of solids. New York: Springer; 1993.
[23] Kanel GI, Razorenov SV, Fortov VE. Shock-wave phenomena and the properties of condensed matter. New York: Springer-Verlag; 2004.
[24] Lysne PC, Boarde RR, Percival CM, Jones OE. Determination of release adiabats and recented Hugoniot curves by shock reverberation techniques. J Appl Phys 1969;40(9):3786–95.
[25] Kondo K, Yasumoto Y, Sugiura H, Sawaoka A. Multiple shock reverberations in a layer structure observed by particle velocity and pressure gauges. J Appl Phys 1981;52(2):772–6.
[26] Ramesh KT. Handbook of experimental solid mechanics. Massachusetts: Springer; 2009.
[27] Meyers MA. Dynamic behavior of materials. New York: John Wiley & Sons; 1994.
[28] Hall CA, Chhabildas LC, Reinhart WD. Shock Hugoniot and release in concrete with different aggregate sizes from 3 to 23 GPa. Int J Impact Eng 1999;23(1):341–51.
[29] Comité Euro-International du Béton. CEB-FIP Model Code 1990. Trowbridge, Wiltshire, UK: Redwood Books; 1993.
[30] Franklin J, Katsabanis T, editors. Measurement of blast fragmentation. Rotterdam: A.A.Balkema Publishers; 1996.
[31] Bischoff PH, Perry SH. Compressive behaviour of concrete at high strain rates. Mater Struct 1991;24(6):425–50.
[32] van Mier JGM. Fracture processes of concrete: assessment of material parameters for fracture models. CRC Press; 1997.